

4-26-2023

Morphological Characterization of Two Transgenic Strategies for Genetic Access to Semilunar Granule Neurons in the Mouse Dentate Gyrus

David T. Rexford

Follow this and additional works at: <https://scholarworks.gvsu.edu/theses>



Part of the [Molecular and Cellular Neuroscience Commons](#)

ScholarWorks Citation

Rexford, David T., "Morphological Characterization of Two Transgenic Strategies for Genetic Access to Semilunar Granule Neurons in the Mouse Dentate Gyrus" (2023). *Masters Theses*. 1086.
<https://scholarworks.gvsu.edu/theses/1086>

This Thesis is brought to you for free and open access by the Graduate Research and Creative Practice at ScholarWorks@GVSU. It has been accepted for inclusion in Masters Theses by an authorized administrator of ScholarWorks@GVSU. For more information, please contact scholarworks@gvsu.edu.

Morphological Characterization of Two Transgenic Strategies for Genetic Access to Semilunar
Granule Neurons in the Mouse Dentate Gyrus

David T. Rexford

A Thesis Submitted to the Graduate Faculty of

GRAND VALLEY STATE UNIVERSITY

In

Partial Fulfillment of the Requirements

For the Degree of

Master's of Health Science

Department of Biomedical Sciences

April 2023

Thesis Approval Form



The signatories of the committee below indicate that they have read and approved the thesis of David T. Rexford in partial fulfillment of the requirements for the degree of Master of Health Science in Biomedical Science.

Chris Pearl April 11, 2023
Christopher Pearl, Thesis committee chair Date

Michael R Williams Feb. 13, 2023
Michael Williams, Committee member Date

Daniel Vogt March 21st, 2023
Daniel Vogt, Committee member Date

Accepted and approved on behalf of the
College of Liberal Arts and Sciences

Dean of the College

4/13/2023

Date

Accepted and approved on behalf of the
Graduate Faculty

Dean of The Graduate School

4/26/2023

Date

Abstract Page

Granule cells (GCs) of the dentate gyrus (DG) have been understood as a homogeneous class of neurons exhibiting a characteristic limited firing pattern. A subtype of GC called a semilunar granule cell (SGC) has been identified exhibiting variant morphology, electrophysiology, and positioning from normal GCs. SGCs represent an emerging novel subpopulation of GCs, however, there is presently no genetic tool to access SGCs separately from normal GCs. To provide access for future *in vivo* studies of this population, we examined two genetic strategies for putative SGC specificity in mouse brain slices. Morphological analysis was performed for quantitative identification of putative SGCs in a total of 822 neurons. Experimental neurons possessed between one and four primary dendrites (PDs) in both strategies. The mean circularity index (CI) of somas from both strategies was .88 . Intersectional strategy somas were found to express 1.95 PDs on average, while enhancer trap strategy somas had an average of 2.2 PDs. 114 dendritic spans were measured in our intersectional strategy, neurons with greater than one PD had 64.5% greater spans than neurons with only one PD. Our enhancer trap strategy for SGC access is tamoxifen-inducible, allowing for temporal control over transgene expression. Our intersectional strategy utilizes the differential co-expression of transgenic populations to specifically access SGCs, allowing for induction scheme variation. Our results suggest these methods may be used to access SGC populations, however, the heterogeneous morphological characterization of SGCs and lack of specific SGC markers in the literature limit confident identification of this population. Our study supplements available literature by providing a large scale manual analysis of individual SGC morphology. These strategies open the possibility for manipulation of the SGC population, such as through inactivation, in order to further explore the relationship of this population to cognitive processing *in vivo*.

Table of Contents

Title Page	1
Approval Page	2
Abstract	3
List of Figures	6
List of Abbreviations	7
Chapter 1: Introduction	
1.1 The Hippocampal Formation.....	8
1.2 The Trisynaptic Circuit.....	9
1.3 Anatomy of the Dentate Gyrus.....	10
1.4 Trisynaptic Pathway.....	11
1.5 Dentate Gyrus Granule Cells.....	11
1.6 Mossy Cells.....	12
1.7 Basket Cells.....	13
1.8 Semilunar Granule Cells.....	13
1.9 Initial SGC Characterization.....	14
Chapter 2: Review of Literature	
2.1 SGC Morphology.....	17
2.2 SGC Gene Expression.....	18
2.3 Developmental Origin of SGCs.....	19
2.4 SGC Location.....	20
2.5 SGC Electrophysiology.....	20
2.6 SGCs & Hilar Barrages.....	22
Chapter 3: Methodology	
3.1 SGC-Specific Dual Transgenic Mouse Models.....	25
3.2 Single Transgene Inducible Cre Model.....	27
3.3 Sectioning and Microscopy.....	28
3.4 Intersectional Strategy Analysis.....	28
3.5 Enhancer Trap Strategy Analysis.....	30
3.6 Statistical Analysis.....	31
Chapter 4: Results	
4.1 Primary Dendrites.....	32
4.2 Dendritic Span.....	32
4.3 Specificity.....	33
4.4 Somas.....	33
Chapter 5: Discussion & Conclusion	
5.1 Dendritic Structure.....	37
5.2 Neurogenesis & Migration.....	38

5.3 Induction Patterns.....	38
5.4 Conclusion.....	39
Bibliography.....	41

List of Figures

Figure 1: Hippocampal Formation Anatomy.....8

Figure 2: The Hippocampal Trisynaptic Circuit.....9

Figure 3: Comparative Morphology & Electrophysiology of SGCs and GCs.....14

Figure 4: Flp/DOG AAV Mechanism.....25

Figure 5: Enhancer Trap Strategy & Intersectional Strategy.....27

Figure 6: Description of Morphological Measurements.....30

Figure 7: Intersectional Strategy Summary.....34

Figure 8: Enhancer Trap Strategy Summary.....35

Figure 9: Intersectional Strategy Statistical Analysis.....36

List of Abbreviations

Abbreviation	Definition
HF	Hippocampal Formation
DG	Dentate Gyrus
CA	<i>Cornu Ammonis</i>
GCL	Granule Cell Layer
ML	Molecular Layer
GABA	γ -aminobutyric acid
GC	Granule Cell
SGZ	Subgranular Zone
abGC	Adult-Born Granule Cell
BrdU	Bromodeoxyuridine
MC	Mossy Cell
IML	Inner Molecular Layer
BC	Basket Cell
SGC	Semilunar Granule Cell
PD	Primary Dendrite
TBI	Traumatic Brain Injury
sIPSC	Spontaneous Inhibitory Post Synaptic Current
PV	Parvalbumin
BAC	Bacterial Artificial Chromosome
KG	Kit GFP
AAV	Adeno-Associated Virus
ET	Enhancer Trap
ER	Estrogen Receptor
HSP	Heat Shock Protein
CI	Circularity Index
SD	Standard Deviation

Chapter 1: Introduction

1.1 The Hippocampal Formation

The hippocampal formation (HF) is a medial temporal lobe structure composed of the dentate gyrus (DG), hippocampal *Cornu Ammonis* (CA) areas CA1, CA2, and CA3, and the subiculum (Figure 1) (Mendoza et al. 2008). The HF receives incoming sensory signaling from multiple brain regions, facilitating its encoding as discrete long-term and working memories (Walker et al. 2010). The HF is associated with research examining memory and learning pathologies and is tightly correlated with temporal lobe epileptogenesis (Clark et al. 2017; Scharfman, 2000; Save et al. 2018). The particular competence of the HF for memory encoding is dependent upon an assembly of distinct cell types found throughout HF regions (GoodSmith et al. 2017). Studies examining prominent populations within this system develop models of cellular memory dynamics and provide insight to future studies aimed at correcting pathologies of memory and learning processes.

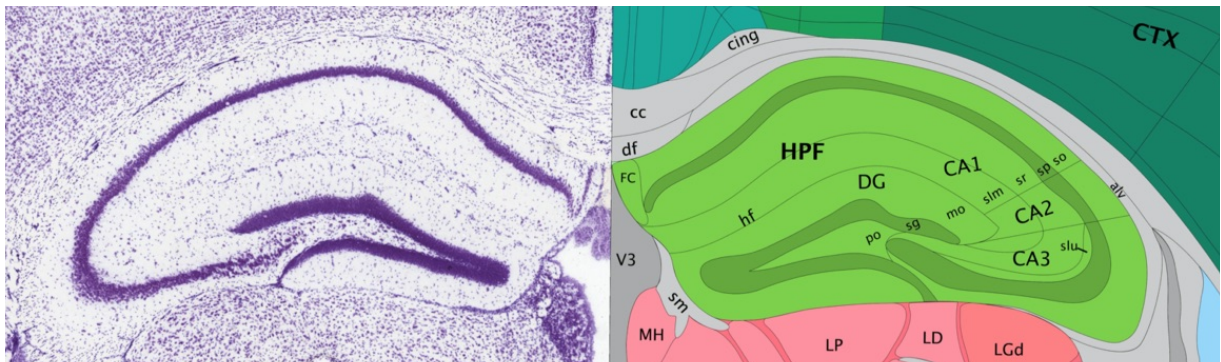


Figure 1. Hippocampal Formation Anatomy Adapted from Allen Brain Atlas (left) Nissl-stained hippocampal formation with (right) mirrored anatomical sketch. Abbreviations: (HPF) Hippocampal Formation; (DG) Dentate Gyrus; (mo) molecular layer of DG; (sg) granule cell layer of DG; (po) polymorphic layer (hilus); (slm) stratum lacunosum-moleculare.

1.2 The Trisynaptic Circuit

Bundles of axons extending between the DG and hippocampal regions CA3 and CA1 compose a prominent HF structure known as the trisynaptic circuit (Figure 2) (Stepan et al. 2012; Basu & Siegelbaum, 2015). The trisynaptic circuit is a pathway receiving the majority of the sensory signaling entering the HF and functions dynamically in processing, storing, and retrieving environmental stimuli as encoded memories (Schmidt et al. 2012; Senzai, 2019). The collaborative functioning of specialized cell types found throughout the circuit effectively store overlapping barrages of sensory data from distinctive environmental contexts into separate, retrievable memories (Woods et al. 2020). Curiously, synapses found in CA3 and CA1 are excitatory and experience excitotoxicity leading to cellular death if sensory inputs entering the circuit are not dampened (Gonzales-Burgos et al. 2009). The DG, termed “the entrance gate to the hippocampus”, contributes to the trisynaptic circuit by acting as a low-throughput center, relaying sensory inputs entering the trisynaptic circuit in discrete and sparse packages to volatile hippocampal synapses (Figure 2) (Ascady et al. 2000; Save et al. 2019; Walker et al. 2010).

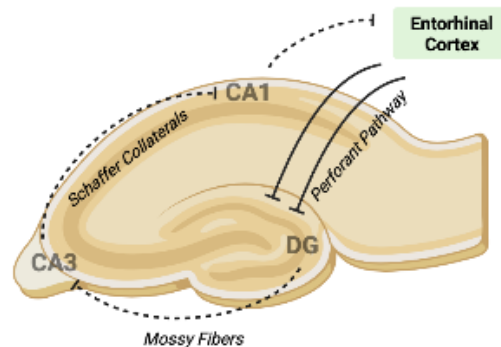


Figure 2. The Hippocampal Trisynaptic Circuit

Schematic created with BioRender software showing excitatory perforant pathway signaling to the DG, limited delivery of signaling from the DG to excitatory synapses in CA3, CA3 schaffer collaterals projecting to excitatory synapses of CA1, and CA1 projecting back to the entorhinal cortex.

The entorhinal cortex bundles environmental stimuli received in the cortex for delivery into the trisynaptic circuit by fibers of the perforant pathway (Figure 2) (Sancho-Bielsa et al. 2012). Perforant pathway fibers terminate at the DG (Figure 2), characterized by an uncommonly forceful intrinsic and circuit-mediated inhibition on its neuronal populations (Hatami et al, 2018). The inhibitory environment and intrinsic properties of DG output neurons leads them to fire sparsely, transmitting data to CA3 and CA1 synapses in a tightly regulated, limited manner (Dengler & Coulter, 2016). The limited propagation of perforant pathway inputs by the DG reduces the sensory bandwidth relayed into the trisynaptic circuit and is necessary for sustaining CA3 and CA1 function (Dengler & Coulter, 2016). Hippocampal memory function is thus clarified by a sum of the individual contributions of constituent HF regions.

1.3 Anatomy of the DG

The DG is divided into three anatomical layers termed the hilus, granule cell layer (GCL), and molecular layer (ML). Of these layers, the hilus is the innermost, the GCL is found in the center, and the ML is the most peripheral (Figure 1) (Walker et al. 2010; Sancho-Bielsa et al. 2012). Throughout all DG layers is a collection of GABAergic interneurons which contribute to the synaptic inhibition within this region (Rovira-Esteban et al. 2020) There is a uniquely high density of interneurons found in the DG hilus (Scharfman, 2016). Interneurons are nearly exclusively located in the central nervous system and contribute to local regulation of sensory and motor signaling (Sik et al. 1997). Interneurons, including those found within the DG, exhibit heterogeneous morphology, physiological traits, and connectivity, however, interneurons can be broadly grouped under the use of GABA as their primary neurotransmitter (Houser et al. 2007). Granule cells (GCs) of the DG are responsible for receiving and projecting DG input and output (Bartos et al. 2001). Their cell bodies are densely packed throughout the GCL and their dendrites

extend into the ML of the DG (Figure 1) (Sancho-Bielsa et al. 2012). The subgranular zone (SGZ) of the DG is a thin layer of the distal hilus that forms a border with the proximal GCL (Christian et al. 2020). In the 1960s, the phenomenon of mammalian adult neurogenesis was discovered for the very first time in the rat SGZ of the DG (Altman & Das, 1965). The SGZ produces adult-born GCs (abGCs) from precursor stem cells which migrate to integrate into DG circuitry throughout adulthood, the SGZ is one of only two regions exhibiting adult neurogenesis in the mammalian brain (Yu et al. 2014; Drew et al. 2013). Tagging GCs with bromodeoxyuridine (BrdU) has revealed early-born GCs to migrate further towards the GCL/ML border while late-born, younger GCs were observed closer to the SGZ (Kaptan & Uzum, 2016).

1.4 Trisynaptic Pathway

The ML of the DG is the first site of perforant pathway projection into the trisynaptic circuit, a region initially damaged in pathologies such as epilepsy and Alzheimer's disease (Henze et al. 2000; Sancho-Bielsa et al. 2012). Stimuli is transmitted out of the DG via the specialized axons of GCs termed "mossy fibers" to the CA3 region of the hippocampus (Figure 2) (Henze et al. 2000). The axons of CA3 output neurons, termed Schaffer collaterals, project to CA1 (Figure 2) (Kaptan & Uzum, 2016). CA1 neurons project back to the entorhinal cortex to complete the trisynaptic circuit (Figure 2) (Xiong et al. 2017). The transmission of perforant pathway signaling by the DG is highly regulated at anatomical and synaptic levels as well as through functionally unique neuronal populations (Faghihi & Moustafa, 2015).

1.5 Dentate Gyrus Granule Cells

DG GCs are glutamatergic cells that fire in a highly controlled, non-spontaneous manner (Jinde et al., 2013; Duffy et al. 2013). GC mossy fiber axons synapse with pyramidal cells and interneurons within the CA3 region of the trisynaptic circuit, a single mossy fiber from one GC

can reach about 15 pyramidal neurons in CA3, 40 to 50 interneurons in CA3, and up to 150 hilar interneurons in the DG via mossy fiber collaterals (Alkadhi, 2019; Christian et al., 2020; Sik et al., 1997). Although DG GCs contact large neuronal populations, their physiological limited firing prevents hyperexcitability within these networks; this sparseness is additionally thought to be critical to normal learning and memory, being related to the capacity to form discrete memories (Senzai et al. 2019).

Because GC mossy fiber axons deliver sensory signaling out of the DG and on to CA3, sparse transmission of perforant pathway inputs to excitable CA regions is dependent on limited activation of GCs. A portion of the inhibitory regulation on GCs is intrinsic, GCs rest at hyperpolarized membrane potentials making them resistant to depolarization (Williams et al. 2007). Granule cells also swiftly adapt in response to depolarizing signaling (Dengler & Coulter, 2016). These properties limit GC excitability to facilitate specific and effective memory encoding; indeed the dysregulation of GC excitability is implicated in the pathogenesis of temporal lobe epilepsy (Althaus & Parent, 2012). In addition to intrinsic regulation, GCs are further regulated by an extensive local network of excitatory and inhibitory inputs.

1.6 Mossy Cells

In addition to receiving sensory inputs within the ML, GCs dendrites are also activated by mossy cells (MCs). MCs are glutamatergic neurons that are characterized by having large complex dendritic spines and large somas (Sun et al. 2017). The cell bodies of MCs are located exclusively in the hilus with monosynaptic connections to GCs in the GCL as well as axons that primarily project to the ipsilateral and contralateral inner molecular layer (IML), the innermost third of the ML (Scharfman & Bernstein, 2015). Recordings from hilar MCs suggest that they generate dense local axon collaterals within the DG hilus where a high density of inhibitory interneurons is found

(Scharfman, 2016). GCs rely on MC-mediated activation, when MCs are inactivated GCs are unresponsive to perforant pathway stimulation (Scharfman, 2016). In addition to mediating GC excitation, MCs also inhibit GCs via their circuit connection to GCs through large networks of GABAergic neurons (Scharfman, 2016; Scharfman, 2018).

1.7 Basket Cells

Basket cells (BCs) are the most common of all GABAergic interneurons found in the DG, inhibiting their target cells (Bartos et al. 2001). These neurons are innervated by MCs and synapse onto GCs, as such, GC inhibition results from MCs activating BCs which in turn inhibit GCs (Scharfman, 2016). BCs exhibit uniquely high frequency firing and activate each other more rapidly than they do GCs, as such, large networks of BCs are quickly activated in response to stimulation and in turn, these interneuron networks functionally inhibit GCs (Bartos et al. 2001; Scharfman, 2016). Through these networks, one BC may reach up to 10,000 GCs (Afrasiabi et al. 2022).

1.8 Semilunar Granule Cells

DG GCs have historically been understood as a homogeneous class of neurons exhibiting tightly controlled, limited firing due to intrinsic and extrinsic regulation (Larimer & Strowbridge, 2010). Studies which examine heterogeneity in GCs have largely amounted to variations during their maturation, which are transient (Wang et al. 2021). Semilunar granule cells (SGCs) are a sub-population of the DG GC, the first electrophysiologic recordings from this population described tremendous variation from historically understood GC functionality and upset long-held understandings of DG circuitry and processing (Williams et al. 2007; Walker et al. 2010; Drew et al. 2013). While SGCs represent an unanticipated sub-population of normal DG GCs, there is presently no gene which selectively defines SGCs from the larger GC population (Afrasiabi et al.

2022). Lack of an established genetic tool to access SGCs presently limits research on this population *in vivo*, where the relevancy of SGC function in a living organism might be examined.

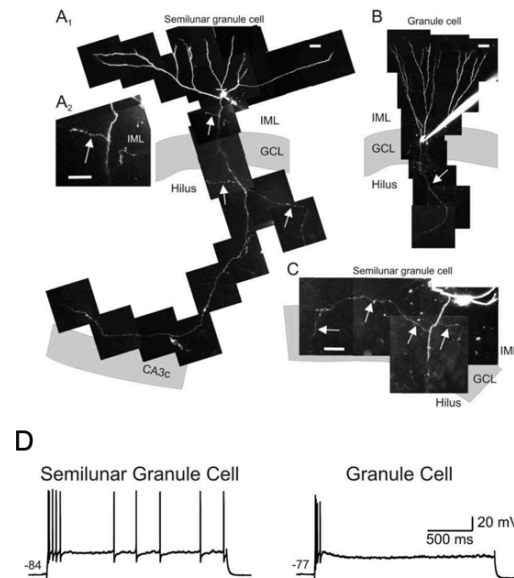


Figure 3. Comparative Morphology & Electrophysiology of SGCs and GCs in Rats.

A₁ Dye-filled SGC showing wide dendritic arborization, semilunar soma shape, axon collaterals in the hilus, to CA3, and in the IML. **A₂** IML axon collateral enlargement. **B** Reconstruction of typical GC. **C** Example of SGC axon collaterals in the ML. **D** *In vitro* responses of SGCs and GCs to 2s depolarizing current steps, performed by Williams and colleagues (2007). Scale bars = 25 microns.

1.9 Initial SGC Characterization

The first study of SGC morphology and electrophysiology was performed by dye-filling patch-clamped cells in hippocampal rat brain slices (Williams et al. 2007). SGCs were observed with polarized dendrites, an axon to the hilus and CA3, and dense dendritic spines like normal GCs, however, this population presented with atypical morphology, location, electrophysiology, and connectivity (Figure 3). SGCs were described to have triangular or semilunar somas (Figure 3C), distinct from spherical GCs, and were found at the border between the GCL and ML (Figure 3A₁), more peripheral than normal GCs. Like GCs, SGCs were observed with axon collaterals to the hilus, however, SGCs were found with additional axon collaterals to the IML and GCL (Figure 3A₂ & 3C). SGCs differ from normal GCs most obviously in their electrophysiology, patch-

clamped SGCs were found to fire multiple action potentials for several seconds following stimulation while GCs only discharged through the first 100ms of the response (Figure 3D). SGCs were found with significantly lower spike frequency adaptation and input resistance than normal GCs, suggesting largely different functions within DG circuitry. Paired cell recordings revealed SGCs to monosynaptically excite MCs and interneurons in the hilus and hilar stimulation revealed that SGCs are likely excited by MC axons. This unique connectivity to MCs and inhibitory interneurons has led to the proposition that SGCs limit activity in the DG by exciting inhibitory populations (Williams et al. 2007; Scharfman et al. 2018; Afrasiabi et al. 2022; Walker et al. 2010).

Prior to this study by Williams and colleagues (2007), GCs of the DG were understood within the field as a homogenous population characterized by limited firing. The discovery of SGCs challenged this understanding, implying that the complexity of DG circuitry exceeds current descriptions. The presence of SGC dendrites in the ML suggests a potential role in sampling perforant path signaling entering the trisynaptic system while their rapid spiking and monosynaptic connections to MCs suggest robust modulation of GC activity and therefore DG output. Here, our team performs morphological characterization of two distinct strategies for GC-independent transgenic SGC specificity in the mouse brain.

Purpose

The purpose of this study is to establish access to SGCs *in vivo* in the mouse brain.

Scope

We sought to examine the spatial distribution and morphology of transgenically designated neuronal populations in the mouse DG to evaluate them for SGC specificity. Our intersectional strategy utilizes the differential expression of designated populations in the Grm2 Cre and KG lines to specify SGCs and our ET strategy explores an inducible, single allele strategy for such access.

Assumptions

We assume the previously described *in vitro* behavior of SGCs indicates robust *in vivo* activity, which may have therapeutic relevance. We also assume our manipulation of transgenes does not cause atypical morphological development in our model populations.

Hypothesis

Our strategies for isolating SGCs will supplement available morphological data on this population and pave the way for future *in vivo* manipulations of SGCs.

Significance

The SGC population exhibits robust involvement in HF processing *in vitro*, our strategies for *in vivo* access to SGCs will allow their investigation in model organisms where the role of SGC in HF-relevant learning and memory processes, as well as their involvement in epileptogenesis and other HF pathologies, may be examined.

Chapter 2: Review of Literature

Following the original characterization of dye-filled SGCs in rats by Williams et al. (2007), subsequent studies have noted cells with SGC-consistent morphology and positioning in mice, rabbits, and primates (Save et al. 2019; Sancho-Bielsa et al. 2012; Gupta et al. 2019). These findings provide support for SGC presence throughout mammalian species; it has been suggested that SGCs may become an attractive population for studying epileptogenesis and seizure disorders in humans, where SGCs have not yet been examined (Williams et al. 2007; Gupta et al. 2012). Although recent studies indicate potential for SGCs as a robust contributor to DG and therefore hippocampal functioning, there remains a lack of an established selective genetic marker to allow *in vivo* SGC access and functional manipulations (Afrasiabi et al. 2022).

2.1 SGC Morphology

The cell bodies of SGCs are described to be a comparable area to normal GCs, however, distorted with a semilunar or half-moon shape (Williams et al. 2007; Save et al. 2019). The dendrites of SGCs, like GCs, stretch peripherally into the ML of the DG (Figure 3A₁) (Williams et al. 2007). SGCs have been reliably observed to have a wider lateral spread of their primary dendrites (PDs) than GC counterparts in both the mouse and rat species (Figure 3A₁), however, there is lack of consistency in the reported range of PDs for SGCs. While GCs generally have one PD and less commonly, two (Gupta et al. 2019; Afrasiabi et al. 2022), SGCs have been described to have between two and five PDs in mice (Save et al. 2019), three or more PDs in mice (Afrasiabi et al. 2022) and in studies examining both GCs and SGCs, SGCs have been identified through exhibiting a higher mean number of PDs than GCs in mice (Rovira-Esteban et al. 2020). SGC primary axons, like GCs, stretch towards the hilus and onto CA3, however, SGCs generate additional axon collaterals within the GCL and ML (Figure 3A, B, & C) (Williams et al. 2007).

Because GCs exhibit variation during development, Gupta et al. (2019) examined the morphology of biocytin-filled SGCs throughout stages of postnatal development in rats (Save et al. 2019). Throughout developmental stages representing infancy, adolescence, and adulthood, SGCs were reliably distinguished from GCs according to their larger soma width, larger dendritic angle, and higher number of PDs (Gupta et al. 2019). Thus, differential comparisons of SGC and GC morphology according to these parameters may be used to reliably distinguish between these cell types.

2.2 SGC Gene Expression

Presently, there is little information available on the genetic profile of SGCs. SGCs express the GC marker *Prox1* in mice and in rats (Erwin et al. 2020; Gupta et al. 2012). SGCs of the mouse DG have also been observed expressing a second GC marker *Pcp4* (Erwin et al. 2020). The expression of multiple GC markers indicates that these neurons likely arise from the same neural progenitors as GCs, however, the bizarre electrophysiology found in the SGC population signifies a distinctive split from the neurogenesis of normal GCs. Interestingly, activity-labeling of neurons in the mouse DG during novel environment exploration was found to preferentially tag neurons with morphology and electrophysiology indicative of SGCs, along with a minority (~20%) of classical GCs (Erwin et al. 2020). Analysis of DG single-cell RNA sequencing datasets revealed a discrete *Penk*-expressing population within a broader collection of GCs that co-labeled with previously activity-labeled SGCs (Erwin et al. 2020). More studies are needed to determine the specificity of the *Penk* gene for the SGC population (Afrasiabi et al. 2022). Of note, diverse novel contexts exhibit preferential labeling of SGC-consistent neurons, suggesting SGCs may be recruited at a higher frequency than normal GCs throughout various behaviors (Erwin et al. 2020).

2.3 Developmental Origin of SGCs

Prior to the discovery of the novel traits displayed by SGCs, GCs were understood as a uniform Prox1-expressing population (Yu et al. 2014). Although SGCs share Prox1 expression with all normal GCs and likely arise from the same neural progenitors, several elements have inferred that SGCs follow a defined split from the neurogenic pathway of normal GCs (Gupta et al. 2019). Seizure-related pathologies have been known to cause migration of GCs, termed ectopic GCs, away from their typical GCL organization (Scharfman et al. 2007). While ectopic GCs are displaced from the GCL, their electrophysiology is consistent with normal GCs, as such, it is unlikely that SGCs represent ectopic GCs owing to their distinctive electrophysiology (Williams et al. 2007). As embryologically and adult-born GC neurons mature, they shift from exhibiting high input resistance as immature neurons to exhibiting low input resistance as mature neurons (Schmidt-Hieber et al. 2004). SGCs are reported with low input resistance in juvenile rats, suggesting that the unique electrophysiology of SGCs is not related to temporal variation in GC behavior occurring during development (Williams et al. 2007). In rodents, GC neurogenesis primarily occurs postnatally (Xu et al. 2020; Save et al. 2019). Several studies have suggested that SGCs arise prior to most GCs during early embryological development. By fate-mapping glutamatergic neurons of the DG with a tamoxifen-inducible Cre mouse line, Save et al. (2019) observed that 40% of GCs tagged on E12.5 belonged to the SGC sub-population. SGCs were also tagged to a lesser extent on E14.5 and E16.5, with minimal postnatal expression. This data suggests that SGCs are preferentially generated during embryonic development, prior to most normal GCs (Save et al. 2019). In DG neurons tagged at developmental time points using electroporation, peak labeling of neurons consistent with SGCs was also observed during early embryonic development at E14.5 (Kerloch et al. 2020). The findings of the above studies support an embryonic origin for

SGCs, separating SGCs from the majority of GCs developmentally, and provide evidence that if adult neurogenesis is present in SGCs, it likely amounts to an insignificant portion of the limited SGC population.

2.4 SGC Location

Although SGCs somas were initially characterized according to their presence at the IML/GCL border, ongoing studies have suggested that the position of SGCs may be largely related to the peripheral migration of GCs during neurogenesis (Williams et al. 2007; Erwin et al. 2020). Because normal GCs are generated postnatally throughout adult life, early-born GCs migrate further towards the peripheral GCL while late-born GCs can be found closer the hilar edge of the GCL (Aguilar-Arredondo et al. 2015). Neurons consistent with the morphology and electrophysiology of SGCs have been observed within the GCL, suggesting that the IML orientation of some SGCs is not an exclusive feature of this population but rather, the embryonic birthdate of this population allows it to reach peripheral regions of the DG during neurological development (Erwin et al. 2020). The discovery of a genetic marker that is homogeneous throughout the entire SGC population would allow for a comprehensive anatomical characterization of this population in order to provide quantitative clarity on the limits of SGC positioning.

2.5 SGC Electrophysiology

While the literature on morphologic and anatomical guidelines for defining SGCs contains inconsistency, their electrophysiologic behavior is strikingly homogenous (Williams et al. 2007). SGCs are similar to GCs in exhibiting a hyperpolarized resting membrane potential and in their large amplitude action potentials (Williams et al. 2007). Although some electrophysiologic parameters are comparable between SGCs and GCs, SGCs differ significantly from GCs in their

input resistance and spike frequency adaptation (Williams et al. 2007; Gupta et al. 2012). Unlike GCs, SGCs display low resistance to incoming signaling as well as slow adaptation to inputs (Gupta et al. 2019). These intrinsic differences lead SGCs to fire persistently in response to depolarizing signaling while normal GCs remain largely inactive (Figure 3D) (Williams et al. 2007; Larimer & Strowbridge, 2010).

The unique electrophysiologic capabilities of SGCs have been observed throughout development in rats (Gupta et al. 2019). SGCs were found to have significantly higher spontaneous inhibitory post-synaptic current (sIPSC) frequencies than age-matched GCs throughout all developmental stages, with a pronounced increase during adolescence. SGCs also displayed a larger amplitude of tonic GABA currents than GCs throughout development with a similar peak at adolescence. Increased expression of extrasynaptic GABA_AR δ receptors are suspected to be the source of increased SGC GABA currents during adolescence as described by Gupta and colleagues (2012; 2019). The expression of GABA_AR δ receptors renders SGCs vulnerable to alcohol while the heightened inhibition of SGCs during adolescence suggests that adolescent alcohol use may uniquely impair SGC functioning.

Dysfunction of the DG IML is closely associated with temporal lobe epilepsy, Gupta and colleagues (2012) created epileptic model rats through inducing a temporal lobe traumatic brain injury (TBI) and investigated the electrophysiologic activity of SGCs during this seizure disorder. In experimental epileptic rats with a TBI, synaptic and tonic GABA currents in SGCs were decreased. Notably, 1 week after injury tonic GABA current amplitudes were significantly increased in GCs while they were significantly decreased in SGCs. The postinjury reduction in inhibition of SGCs may augment hyperexcitability in this population, suggesting SGCs could be a

component of DG hyperexcitability observed in cases of temporal lobe epilepsy and autism (Takarae & Sweeney, 2017; Gupta et al. 2012; Tamir et al., 2017;).

2.6 SGCs & Hilar Barrages

The atypical electrophysiology of SGCs indicates that this population likely serves an independent function from classical GCs in the DG. Perforant pathway signaling is traditionally thought to activate GC dendrites in the ML, which activate hilar MCs that either excite GCs directly or inhibit them through complex patterns of heterogeneous interneuron activation (Scharfman, 2018). Although this pathway is well-known, studies of MC effects on GC behavior yield conflicting results that lack a clear interpretation (Scharfman, 2016). *In vitro* stimulation of the perforant pathway in rat hippocampal slice preparations was found to evoke a sustained inhibitory DG response described as a hilar barrage (Larimer & Strowbridge, 2010). This hilar up-state or barrage produced inhibition of DG GCs for a period exceeding ten seconds. This *in vitro* model of DG perforant pathway signal processing suggests that this region dampens incoming excitatory stimuli from the entorhinal cortex through a robust mechanism driving the firing of inhibitory hilar neurons. Interestingly, stimulation of the perforant pathway was found to cause hilar barrages in slices with CA3 or the entorhinal cortex removed. As such, the origin of this persistent inhibitory activity in hilar neurons was confined within intrinsic DG circuitry.

In vitro perforant pathway-induced hilar barrages in rat hippocampal brain slices were found to inhibit the majority (68%) of GCs while only 22% of SGCs were inhibited (Larimer & Strowbridge, 2010). The GCs which were not inhibited during hilar excitation were mostly unresponsive, with only 2/25 displaying weak depolarization. Perforant pathway-evoked hilar barrages were silenced when SGC plateau potentials were abolished with nickel administration and out of the five sources of excitatory input to hilar cells, SGCs were the only population required

to cause a hilar barrage (Larimer & Strowbridge, 2010). The unique persistent firing of SGCs observed by Williams et al. (2007) was reproduced through perforant pathway-evoked hilar barrages and the duration of persistent firing in SGCs tightly corresponded to the length of hilar barrages (Larimer & Strowbridge et al. 2010). Due to the intimate association between SGC activity and hilar barrages seen in hippocampal slice experiments, it has been proposed that SGCs are the initial source of the hilar up-state observed by Larimer & Strowbridge (2010) (Scharfman, 2018). In this mechanism, the entorhinal cortex projects perforant pathway inputs onto SGC dendrites in the ML, causing the persistent firing of SGCs seen *in vitro* which in turn activates hilar MCs and interneurons, inducing a hilar barrage which functionally dampens GC firing in order to optimize DG output (Scharfman, 2016). Indeed, early 2-photon microscopy of the rat DG revealed SGC axons to contact MC dendrites and later studies in mice have revealed SGC to make synaptic contact with inhibitory DG interneurons within the GCL and hilus (Williams et al 2007; Rovira-Esteban et al. 2020). The results of these studies suggest that further characterization of SGCs within the DG circuit may provide clarity in light of ongoing confusion over the nature of MC activity within the DG (Scharfman, 2016).

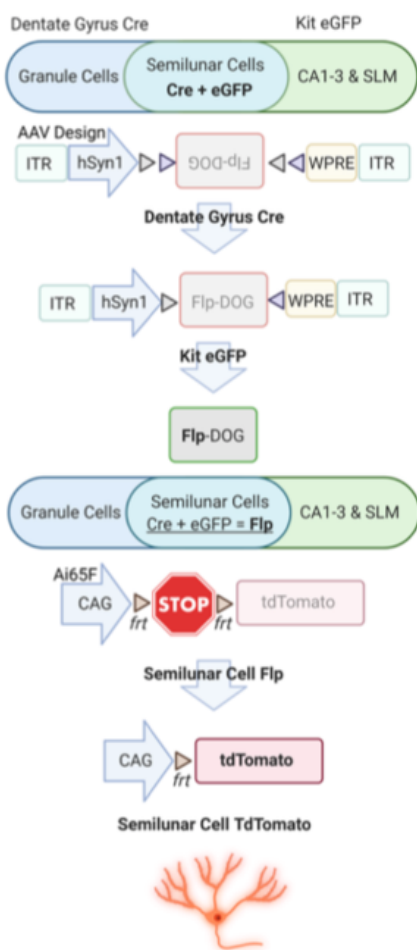
Parvalbumin (PV) positive interneurons are a heterogenous population of GABAergic interneurons that are found throughout all three DG layers and contribute to the local inhibition of its neuronal populations (Afrasiabi et al. 2022). While MCs, normal GCs, and other afferents were not found to provide significant glutamatergic input onto these inhibitory PV interneurons, biocytin-filled neurons consistent with SGCs have been observed making contact with PV interneurons in the IML, GCL, and the hilus (Rovira-Esteban et al. 2020). The finding that SGCs provide glutamatergic input onto PV interneurons of the DG while other notable DG populations do not is evidence that SGCs possess executive control over the heightened interneuron activity

that dampens GC firing. In corroboration with reports of SGCs exciting MCs, evidence of glutamatergic input from SGCs onto PV interneurons throughout the DG place this newly recognized sub-population of GC in a privileged position to alter the field's understanding of DG processing (Larimer & Strowbridge, 2010; Walker et al. 2010; Rovira-Esteban et al. 2020).

Chapter 3: Methodology

3.1 SGC-specific Dual Transgenic Mouse Models

The central goal of these experiments was to characterize transgene expression in mice towards identifying a strategy that will allow for the targeting of SGCs separately from normal GCs within the DG. Previously, the lab of Michael Williams examined transgenic mice to identify those with potential enrichment of transgenes in SGCs vs GCs.



The Grm2 Cre mouse line constitutively expresses Cre driven by a bacterial artificial chromosome (BAC) in mature GCs, SGCs, and a small subset of CA cells. Separately, the lab has made the observation that, within the hippocampal formation, a Kit GFP (KG) transgenic mouse line expresses GFP in CA3, CA2, and CA1 and SGCs, but not GCs (Figure 4). In KG, a BAC drives the expression of GFP under control of the kit promoter and other regulatory elements. We crossed KG hemizygous mice with an Ai65 TdTomato Flp reporter mouse in order to visualize future Cre-on Flp/DOG-infected neurons (The Jackson Laboratory). Eight-week old adult offspring were bred with adult Grm2 Cre hemizygous mice. These triple-positive offspring generally express Cre and GFP only in

Figure 4. Fip/DOG AAV Mechanism

Biorender schematic of intersectional strategy showing transgene-designated populations, AAV design, AAV recombination, and activation of Flp recombinase. Abbreviations: inverted terminal repeats (ITR), human synapsin-1 (hSyn1), woodchuck post-hepatitis response element (WPRE).

the SGC population (Figure 4). Following this cross, we stereotaxically injected the left dentate gyrus of 8-week-old offspring with a replication defective adeno-associated virus (AAV) expressing, in a Cre-On fashion, GFP-dependent Flp (Flp/DOG) under isoflurane anesthesia (Figure 4 & Figure 5) (Fricano-Kugler CJ et al., 2016). Thus, these animals express Flp recombinase only in cells that have GFP as well as Cre (Figure 4) (Tang et al., 2016). All animals were housed under standard conditions with ad libitum access to feed. Animals (Grm2/KG/Flp-DOG/Ai65) were then euthanized at 9 weeks by intraperitoneal injections of tribromoethanol and brains were fixed by transcardial perfusion one week after the last injection with a pH 7.4 phosphate-buffered saline containing 4% sucrose, followed by a 4% paraformaldehyde based fixative in the same solution. Brains were carefully dissected, postfixed overnight, and then sectioned in the coronal plane at 100 microns for microscopic evaluation. Animal care protocols and procedures were reviewed and approved by a Michigan State University IACUC.

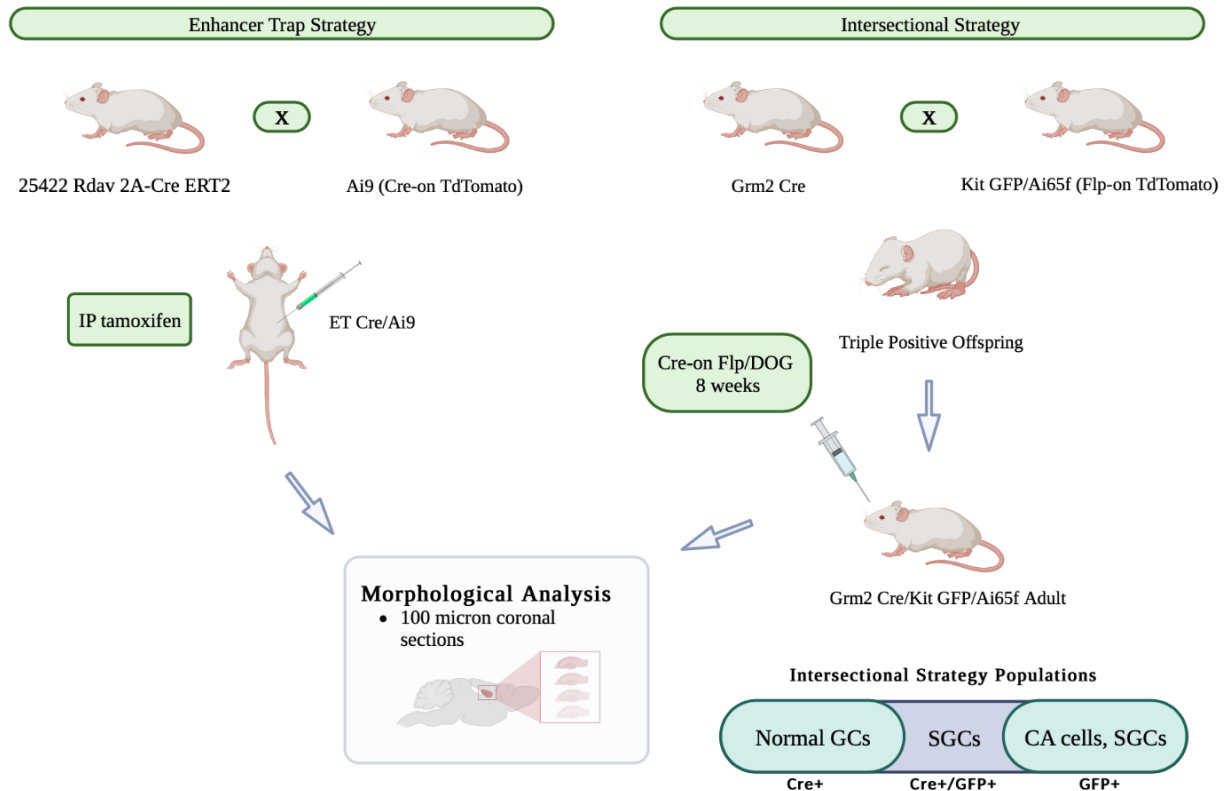


Figure 5. Enhancer Trap Strategy & Intersectional Strategy
Schematic created using BioRender showing enhancer trap strategy (left) and intersectional strategy (right).

3.2 Single Transgene Inducible Cre Model

In addition to our strategy of genetically accessing SGCs independently from GCs via the differential co-expression of two transgenes, we have also performed a limited characterization of the expression of a hemizygous tamoxifen-inducible Cre lineage, ET (Enhancer Trap) Cre ERT2 25422 (Brain Atlas). Upon observing a gross anatomical characterization of Cre expression by the Allen Brain Atlas, these ET Cre mice were found to express Cre specifically in cells located at the border between the GCL and IML where SGCs were initially described. Whole genome sequencing performed by the lab of Michael Williams revealed the presence of the enhancer trap sequence at only one location within the mouse genome. In ET Cre mice, Cre is found in the cytoplasm bound to an estrogen receptor (ER) and a heat shock protein (HSP). When tamoxifen is

administered, it binds the ER and causes the dissociation of the HSP from the complex, activating Cre by allowing it to enter the nucleus and interact with LoxP-flanked sites.

If the ET Cre ERT2 25422 lineage is found to designate SGCs independently from GCs with high specificity, this population would represent an attractive, simple strategy for SGC genetic access. Further, ET Cre mice enable variation in induction schemes as well as temporal control, allowing opportunity for additional developmental studies on SGCs. Ai9 TdTomato Cre reporter mice were crossed to the ET Cre line in order to fluorescently label cells expressing Cre (Figure 5). Offspring were then genotyped and those expressing Cre and TdTomato transcripts in a homozygous or heterozygous fashion were given intraperitoneal injections of 10 mg of tamoxifen per mL of a 95% corn oil 5% ethanol solution at 100 microliters every other day 3 times. Perfusion was performed 1-3 weeks after the final tamoxifen injection, using the same procedure as with the intersectional strategy mice (Fricano-Kugler CJ et al., 2016).

3.3 Sectioning and Microscopy

Brain slices were generated with a Leica Vibratome using a section thickness between 50 and 100 microns. Brain slices, in some cases, were stained with DAPI to label nuclei and cover slipped with a fade resistant mountant, such as Prolong Gold. Images were generated on a Zeiss LSM800 Laser Scanning Confocal Microscope; DAPI fluorescence was stimulated with a 405nm laser, GFP with a 488nm laser, and TdTomato with a 561nm laser. Fluorescence was collected using a 20x air objective lens onto a GaAsP detector, 2x frame averaging was used in order to reduce image noise.

3.4 Intersectional Strategy Analysis

Using ImageJ software, the somas of RFP+ neurons were traced using the polygon tool in order to obtain a circularity index (CI), RFP intensity, and soma ROIs were displaced to the slice

background, local to each ROI, in order to generate a background subtracted RFP intensity for each RFP+ neuron (Figure 6D). In order to determine Flp/DOG efficiency, all GFP+ cells in each image stack were marked as ROIs using the ImageJ multi-point tool. RFP+ soma ROIs were analyzed for the co-expression of GFP (Figure 6E) to justify the efficiency of our AAV, the proportion of all GFP+ somas that were both RFP+ and GFP+. Further, each RFP+ cell was examined qualitatively for a PD count and all RFP+ cells with complete dendrites were analyzed using the line tool to measure dendritic arborization (Figure 6F). In cells with one PD, a line ROI was extended 50 microns from the initial dendritic bifurcation point of the PD and a perpendicular line was placed between each lateralmost dendrite and measured in microns to determine dendritic span. In cells with more than one PD, a line was extended 50 microns from the center of the RFP+ soma and a perpendicular line ROI was suspended between each lateralmost dendrite for measurement (Figure 6F). Span ROIs were labeled according to the respective ROI number from previously generated RFP soma ROIs in order to associate dendritic span with other measurements. Finally, the GFP intensity of each RFP+ cell was measured in the green channel using the corresponding RFP soma ROI, as well as local GFP background intensity to obtain a background subtracted GFP intensity for each RFP+ cell (Figure 6E).

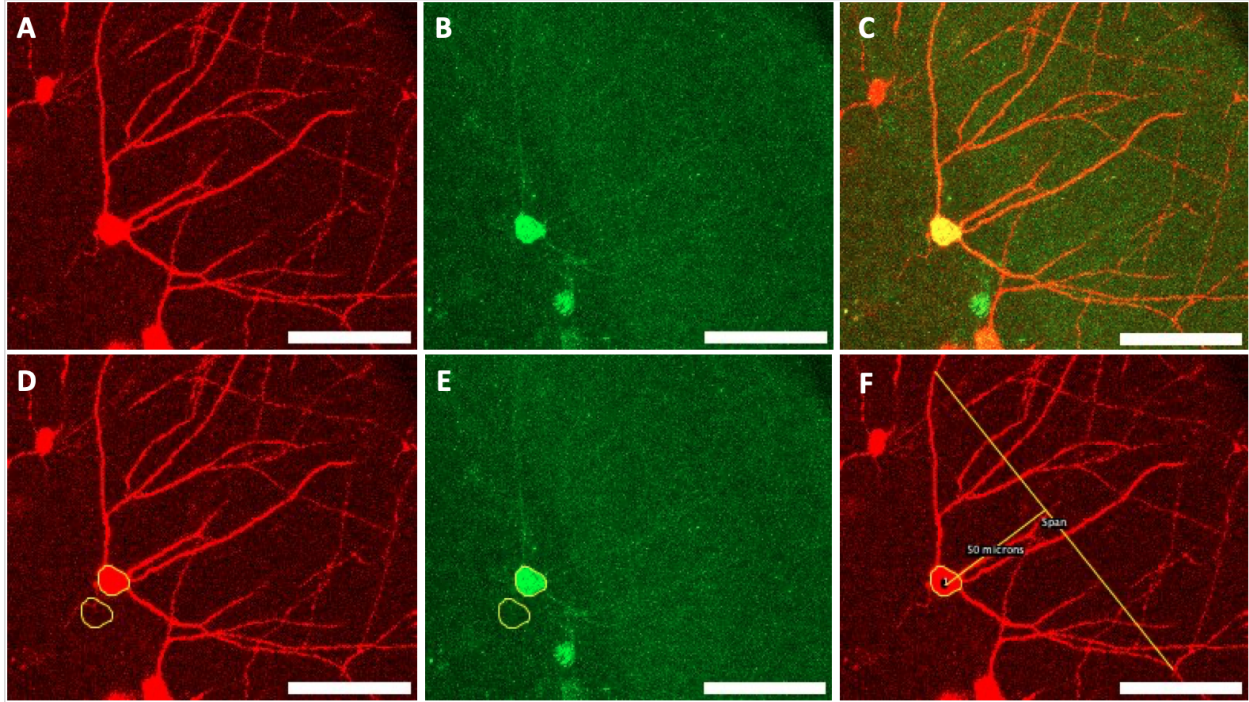


Figure 6. Description of Morphological Measurements

A RFP expression of intersectional strategy soma. **B** GFP expression of same intersectional strategy soma. **C** Composite overlay of RFP and GFP channels. **D** Soma ROI and background displaced soma ROI (RFP). **E** Same ROI as with **D** measured in GFP channel. **F** demonstration of span measurements. All images are a local max projection of z-slices containing ROI morphology. Scale bar = 50 microns.

3.5 Enhancer Trap Analysis

As with our intersectional strategy, RFP+ neurons from our ET Cre ERT2^{KG}/Ai9 were traced using the ImageJ polygon tool yielding area, CI ($4\pi \text{ area}/\text{perimeter}^2$), and intensity. RFP+ soma tracings were displaced to the local background in order to generate a background subtracted intensity for RFP+ neurons. RFP+ somas were qualitatively examined by an observer for PDs and totals were added to corresponding ROI data tables; neurons with unclear dendrites ($n = 10$) were not included in the dataset.

3.6 Statistical Analysis

Statistical analysis was performed to identify variation within our intersectional strategy population. Intersectional strategy somas were grouped by exhibiting one PD or greater than one PD and separately, analyzed as distinct RFP only and RFP/GFP expressing populations. Various two-sample t-tests were performed using Welch's correction in order to identify significant differences between various study parameters.

Chapter 4: Results

4.1 Primary Dendrites

Qualitatively, an observer performed manual analysis of confocal z-stacks to count the number of PDs of designated neurons (Figure 7B). Out of the 708 intersectional strategy RFP+ neurons, 67 lacked sufficient dendritic resolution and were omitted from the analysis. 641 neurons were analyzed for PDs (Figure 6F). Among this population, 207 neurons were found with 1 PD and 434 neurons were observed with greater than 1 PD (Figure 7D), 68% of the population. In our enhancer trap strategy, ten neurons lacked sufficient dendritic resolution and were omitted from the analysis. Out of 114 neurons analyzed for PDs in the enhancer trap strategy, 23 were found with one PD and 91 were observed with greater than 1 PD, 80% of the population. Using an two-sample t-test with Welch's correction, a significant difference in the number of primary dendrites was determined between somas labeled as RFP+ ($n = 203$, $\text{mean}_{\text{PD}} = 1.71$, $\text{SD} = .82$) and RFP+/GFP+ ($n = 439$, $\text{mean}_{\text{PD}} = 2.05$, $\text{SD} = .78$) with a p -value < 0.0001 (Figure 9B).

4.2 Dendritic Span

110 RFP+ cells from our intersectional strategy with complete dendritic arbors were identified and analyzed for dendritic span (Figure 6F). In cells with one PD, the average span was found at 54.8 microns. RFP+ cells with more than one PD yielded an average span of 85.0 microns, 64.5% greater than in RFP+ cells with one PD (Figure 7E). A two-sample t-test was performed on the spans of neurons with 1 PD and > 1 PD demonstrating a statistically significant increased span in neurons with >1 PD ($n = 88$, $\text{mean}_{\text{span}} = 84$ microns, $\text{SD} = 28$) when compared to 1 PD neurons ($n = 22$, $\text{mean}_{\text{span}} = 55$ microns, $\text{SD} = 16$) (Figure 7E). However, there was no statistically significant difference in span between RFP+ only ($n = 24$, $\text{mean}_{\text{span}} = 73$ microns, $\text{SD} = 30$) and RFP+/GFP+ ($n = 86$, $\text{mean}_{\text{span}} = 80$ microns, $\text{SD} = 28$) populations, with a p -value > 0.05 (Figure 9C).

4.3 Specificity

Specificity was measured as the proportion of all GFP expressing cells that were infected with our Flp/DOG virus (Figure 7C). Cells were qualitatively recorded by an observer as being GFP+, RFP+, or both GFP+ and RFP+ (GFP+/RFP+) and this data was quantitatively supported through the measured soma intensities of corresponding neurons from red and green channels (Figure 6D & E; Figure 9A). An unpaired t-test with Welch's correction was performed to validate a significant difference in GFP expression between populations labeled as RFP+ only ($n = 253$) and RFP+/GFP+ ($n = 456$). The mean GFP intensity from RFP+ only neurons was 54 and the mean GFP intensity from RFP+/GFP+ neurons was 725 with a difference between means of 671 and a standard deviation of 38.4 with $p < 0.0001$. Specificity ranged from 64.9% to 11.3%, with a mean of 32% across all three animals. Cases of GFP independent Flp/DOG activity were observed (i.e. RFP+ cell without observable GFP presence). Out of 709 intersectional strategy neurons analyzed for RFP and GFP expression, 35.9% were found to be RFP+ only.

4.4 Somas

In order to promote consistency with other morphological characterizations of SGCs, RFP+ somas were analyzed according to their area and CI through soma tracing of RFP somas with the ImageJ polygon tool (Figure 6D & E). RFP+ intersectional strategy somas were found to have a mean CI of .88 and an area of 105 cubic microns. Enhancer trap somas were found to have a mean CI of .88 and an area of 85.97 cubic microns. Enhancer trap somas varied in their CI between a maximum of .97 and minimum of .73, intersectional strategy somas varied in their CI between .98 and .64.

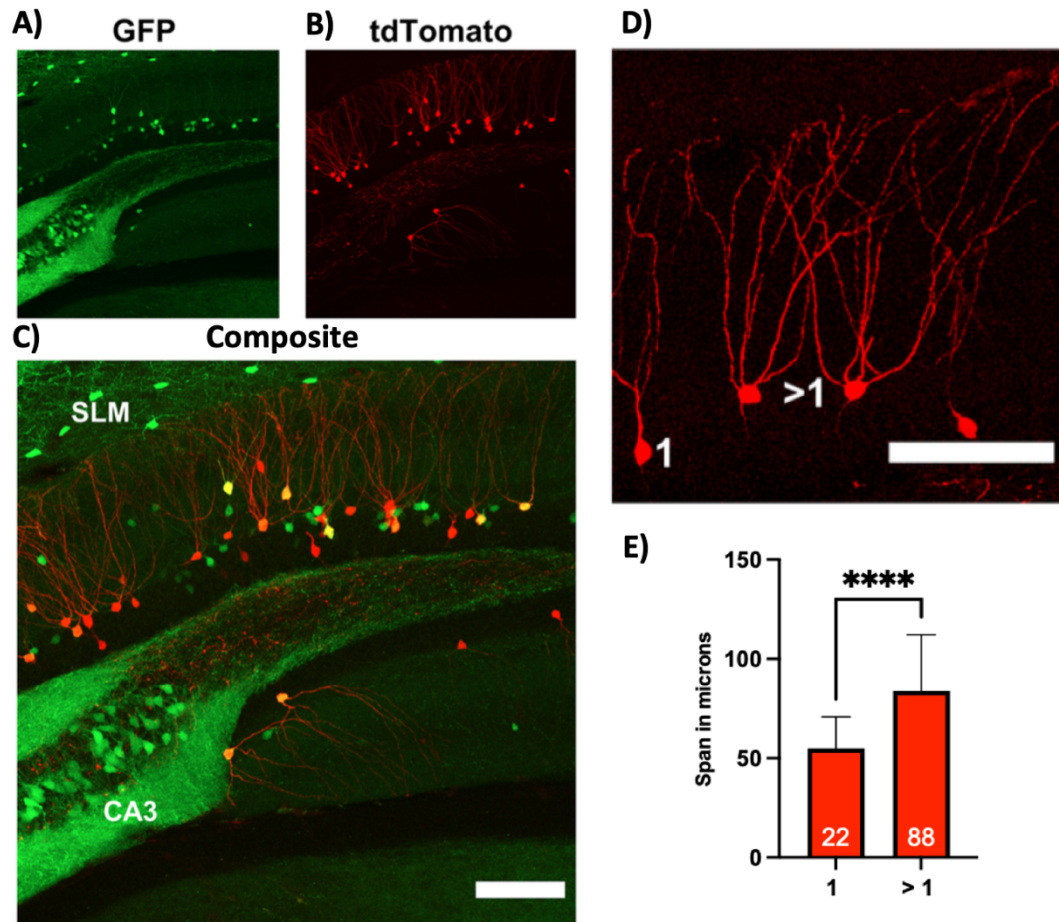


Figure 7. Intersectional Strategy Summary

A GFP expression from Kit eGFP mouse, note lack of RFP in CA populations. **B** RFP expression via our Cre-on Flp/DOG. **C** composite overlay of GFP and RFP channels (scale bar = 100 microns). **D** Demonstration of dendritic variation from intersectional strategy neurons (scale bar = 100 microns). **E** Two-sample t-tests of intensity and span results grouped by PD count. **A**, **B**, & **C** max projection of all z-slices for visualization of expression. **D** local max projection of ROI-containing z-slices.

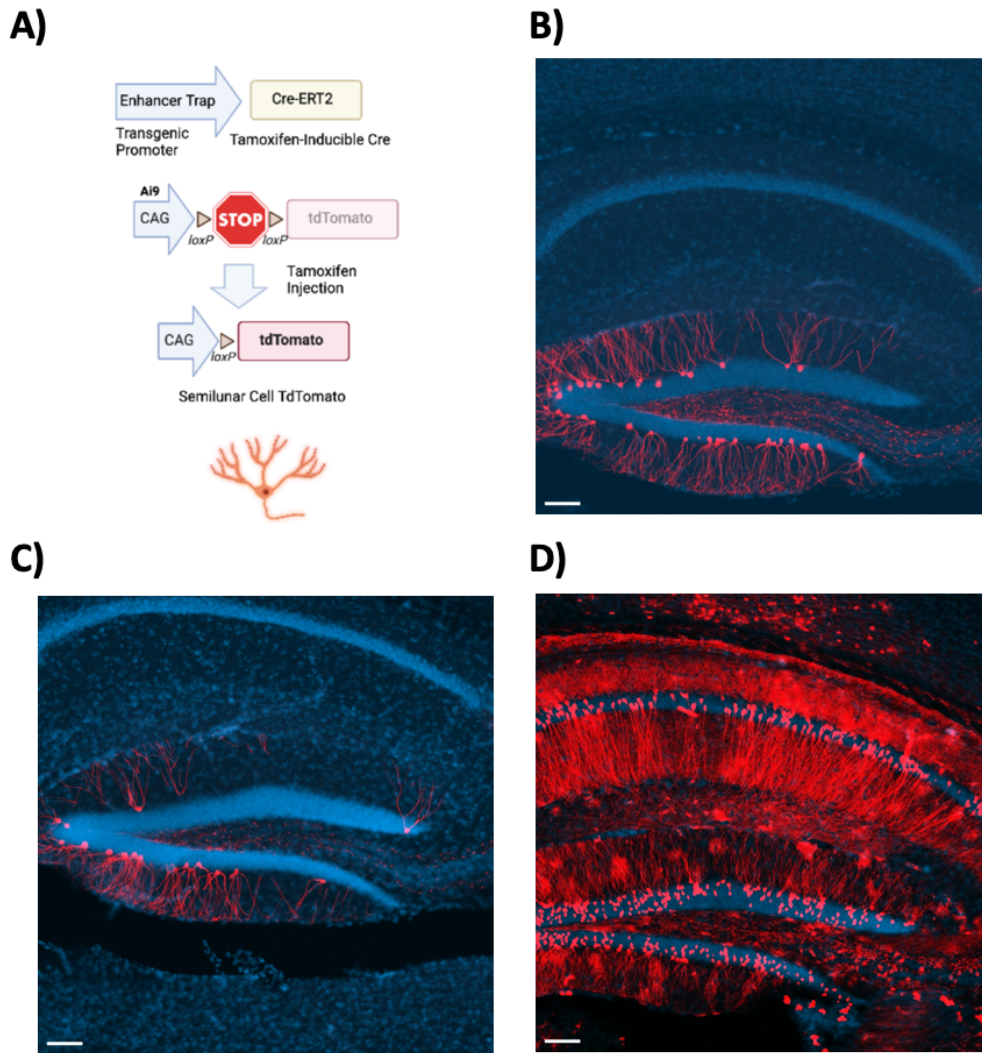


Figure 8. Enhancer Trap Strategy Summary

A Enhancer Trap recombination mechanism. **B** Mid-density (ideal) expression from ET promoter. **C** Low density expression. **D** High density expression. Scale bars = 100 microns.

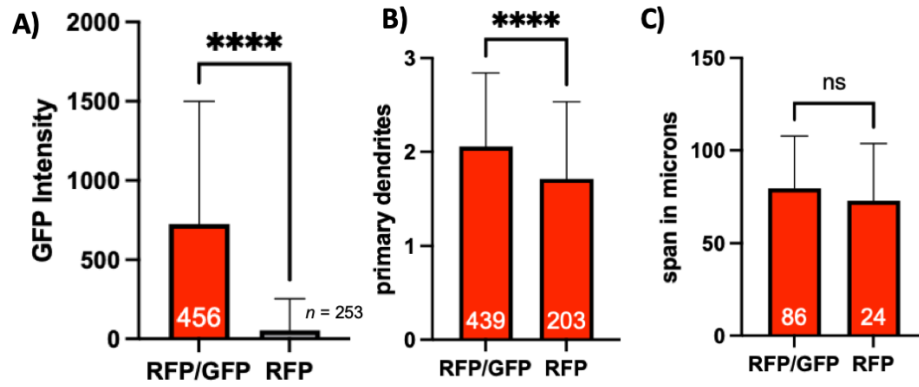


Figure 9. Intersectional Strategy Statistical Analysis

A Representation of GFP intensity among neurons qualitatively designated as RFP+ or RFP+/GFP+. **B** Representation of statistically significant variation in primary dendrites between RFP+ & RFP+/GFP+ populations. **C** Chart showing no statistical difference in span between RFP+ & RFP+/GFP+ populations.

Chapter 5: Discussion & Conclusion

The aberrant electrophysiologic behavior of SGCs clearly distinguishes them from normal GCs, however, performing measurements on individual neurons is time intensive and is not associated with an ability to manipulate these populations at large scale or *in vivo*. Here, we interpret the results of two strategies for transgenic SGC access in terms of the available body of literature on SGCs.

5.1 Dendritic Structure

Through the analysis of 822 manually traced putative SGC somas, 20% of ET somas and 32% of intersectional strategy somas had only one PD (Figure 7E). These results may signify the presence of normal GCs within our study populations, however, they also raise the possibility that SGCs display heterogeneous numbers of PDs. For example, the SGC population may sprout additional dendrites through the course of development in order to establish contact with new adult-born GCs or, perhaps there is an extrinsic regulation which encourages SGC PD proliferation. Outside of PDs, studies point towards SGCs possessing a characteristically wider dendritic arborization than GCs (Gupta et al. 2012). Neurons from our intersectional strategy with greater than one PD had 65% wider spans than neurons with only one PD (Figure 7E). As such, our intersectional strategy may also have selected a portion of GCs. There was no statistical difference in span between RFP+ only neurons and RFP+/GFP+ neurons (Figure 9C). Because morphology was not a qualifying factor for inclusion into our study population our genetic strategies are well-situated to engage with potential morphological heterogeneity in the SGC population. The available literature lacks consensus on a rigid range of PDs for SGCs and our results raise the possibility that SGCs display heterogenous numbers of PDs, including one.

5.2 Neurogenesis and Migration

The progressive neurogenesis of GCs throughout adulthood makes the DG a novel region, however, quantitative evidence of whether or not SGCs undergo this process is lacking. SGC production has been observed to peak at E14.5 in mice, however, no studies have been performed determining the extent of potential SGC production through adulthood (Kerloch et al. 2019; Save et al. 2018). While background staining allows for low resolution visualization of the anatomical layers of the DG, our team did not perform measurements of SGC positioning. Neurons with SGC-consistent morphology were qualitatively observed in high density around the IML/GCL border with expression to a lesser extent within the GCL in both strategies (Figure 7C & Figure 8 B & C). Our findings of putative SGCs in the GCL is in agreement with the recent proposition that SGCs are not entirely restricted to the IML (Gupta et al. 2019; Erwin et al. 2020). If SGCs migrate in a similar fashion to GCs, cases of SGC expression within the GCL could represent part of the insignificant collection of postnatal SGCs. In this description, SGCs typically migrate more peripherally than traditional GCs, closer to the GCL/IML border, as a result of their early birth date rather than due to intrinsic cellular programming. Studies are needed to precisely define the anatomical borders of SGC positioning.

5.3 Induction Patterns

Variation in efficiency and specificity were observed throughout our intersectional strategy sections. Induction schemes may be adjusted to accommodate methods, for example, high-titer Flp/DOG yields high-intensity overlapping expression and is poorly suited for precise morphological measurements on individual cells. Studies on the behavioral effects of SGC silencing may optimize induction schemes for SGC selectivity in order to minimize variables from silencing additional populations. Reducing Flp/DOG titers may also reduce the likelihood of GFP-

independent Flp/DOG activity, as was seen in our intersectional strategy. Tang et al. (2015) described a similar phenomena with their CRE-DOG^{OPT}, a GFP-dependent Cre recombinase. Cases of Cre activity without observable GFP were suspected to be a result of GFP fluorescence below the visualization threshold but sufficient to induce DOG activity, which requires minimal levels of GFP. As such, neurons that were RFP+ only may have exhibited temporal variation in their intensity or pattern of GFP expression, leading to Flp/DOG activity with GFP levels unable to be visualized. There was no statistically significant difference in dendritic span measurements between the RFP+ only and RFP+/GFP+ populations, suggesting that the RFP+ only neurons also display the wide arborization described in SGCs (Figure 9C).

The ET Cre line is attractive due to its designation of the SGC population with a single promoter and furthermore allowing temporal control over Cre expression. There is ample room within the ET strategy for induction scheme variation, however, throughout experimental induction scheme manipulation expression patterns were unpredictable. In cases of optimized labeling, the ET transcript appears to label the SGC population with high specificity (Figure 8B). however, our team was unable to determine an induction scheme yielding consistent expression (Figure 8B, C, & D). Due to animal handling during IP injections, it is possible that a stress response element or other exogenous factor may drive the enhancer trap promoter without Cre recombinase activity, resulting in broad expression extending outside the DG (Figure 8D). Future investigation into the mechanism of this particular ET transcript may produce reliable SGC specificity (Figure 8B).

5.4 Conclusion

Our manual analysis of 832 neurons has suggested that the SGC population may be more diverse in structure and position than was initially proposed. Presently, establishing quantitative

limits on SGC heterogeneity is necessary in order to accurately characterize this novel DG GC subpopulation. Although SGCs seem to consistently display a higher average number PDs than GCs with wider arborizations, it remains to be determined how many or how few PDs SGCs may possess as a population. SGCs may also be more dispersed throughout the DG than their original characterization at the IML/GCL border, possibly reflecting a preferential neurogenesis during early embryonic development with limited postnatal neurogenesis. Electrophysiologic recordings can clearly differentiate SGCs from GCs, however, a specific genetic marker is needed to explore the structural functional relationship of the extraordinary SGC population to DG circuitry *in vivo*. Future studies may benefit from our morphologically justified methods for transgenic SGC access in terms of silencing or manipulating this population through the use of these strategies.

Bibliography

- Acsady, Laszlo, Istvan Katona, Francisco J. Martinez-Guijarro, Gyorgy Buzsaki, and Tamas F. Freund. “Unusual Target Selectivity of Perisomatic Inhibitory Cells in the Hilar Region of the Rat Hippocampus.” *Journal of Neuroscience* 20, no. 18 (2000): 6907–19.
<https://doi.org/10.1523/JNEUROSCI.20-18-06907.2000>.
- Afrasiabi, Milad, Akshay Gupta, Huaying Xu, Bogumila Swietek, and Vijayalakshmi Santhakumar. “Differential Activity-Dependent Increase in Synaptic Inhibition and Parvalbumin Interneuron Recruitment in Dentate Granule Cells and Semilunar Granule Cells.” *The Journal of Neuroscience* 42, no. 6 (February 9, 2022): 1090–1103.
<https://doi.org/10.1523/JNEUROSCI.1360-21.2021>.
- Aguilar-Arredondo, Andrea, Clorinda Arias, and Angélica Zepeda. “Evaluating the Functional State of Adult-Born Neurons in the Adult Dentate Gyrus of the Hippocampus: From Birth to Functional Integration.” *Reviews in the Neurosciences* 26, no. 3 (2015): 269–79.
<https://doi.org/10.1515/revneuro-2014-0071>.
- Alkadhi, Karim A. “Cellular and Molecular Differences Between Area CA1 and the Dentate Gyrus of the Hippocampus.” *Molecular Neurobiology* 56, no. 9 (2019): 6566–80.
<https://doi.org/10.1007/s12035-019-1541-2>.
- Althaus, Alison L, and Jack M Parent. “Pten-Less Dentate Granule Cells Make Fits.” *Neuron* 75, no. 6 (2012): 938–40. <https://doi.org/10.1016/j.neuron.2012.09.008>.
- Altman, Joseph, and Gopal D. Das. “Autoradiographic and Histological Evidence of Postnatal Hippocampal Neurogenesis in Rats.” *The Journal of Comparative Neurology* 124, no. 3 (June 1965): 319–35. <https://doi.org/10.1002/cne.901240303>.

- Bartos, Marlene, Imre Vida, Michael Frotscher, Jorg R. P. Geiger, and Peter Jonas. "Rapid Signaling at Inhibitory Synapses in a Dentate Gyrus Interneuron Network." *Journal of Neuroscience* 21, no. 8 (2001): 2687–98. <https://doi.org/10.1523/JNEUROSCI.21-08-02687.2001>.
- Basu, Jayeeta, and Steven A. Siegelbaum. "The Corticohippocampal Circuit, Synaptic Plasticity, and Memory." *Cold Spring Harbor Perspectives in Biology* 7, no. 11 (2015): a021733. <https://doi.org/10.1101/cshperspect.a021733>.
- Christian, Kimberly M., Guo-li Ming, and Hongjun Song. "Adult Neurogenesis and the Dentate Gyrus: Predicting Function from Form." *Behavioural Brain Research* 379, no. Journal Article (2020): 112346. <https://doi.org/10.1016/j.bbr.2019.112346>.
- Clark, Caron A. C., Fabian Fernandez, Stella Sakhon, Goffredina Spanò, and Jamie O. Edgin. "The Medial Temporal Memory System in Down Syndrome: Translating Animal Models of Hippocampal Compromise." *Hippocampus* 27, no. 6 (2017): 683–91. <https://doi.org/10.1002/hipo.22724>.
- Dengler, C. G., and D. A. Coulter. "Normal and Epilepsy-Associated Pathologic Function of the Dentate Gyrus." *Progress in Brain Research* 226, no. Journal Article (2016): 155.
- Drew, Liam J., Stefano Fusi, and René Hen. "Adult Neurogenesis in the Mammalian Hippocampus: Why the Dentate Gyrus?" *Learning & Memory (Cold Spring Harbor, N.Y.)* 20, no. 12 (2013): 710–29. <https://doi.org/10.1101/lm.026542.112>.
- Duffy, Aine M., Michael J. Schaner, Jeannie Chin, and Helen E. Scharfman. "Expression of C-fos in Hilar Mossy Cells of the Dentate Gyrus in Vivo." *Hippocampus* 23, no. 8 (2013): 649–55. <https://doi.org/10.1002/hipo.22138>.
- Erwin, Sarah R., Weinan Sun, Monique Copeland, Sarah Lindo, Nelson Spruston, and Mark S. Cembrowski. "A Sparse, Spatially Biased Subtype of Mature Granule Cell Dominates

Recruitment in Hippocampal-Associated Behaviors.” *Cell Reports* 31, no. 4 (April 2020): 107551. <https://doi.org/10.1016/j.celrep.2020.107551>.

Faghihi, Faramarz, and Ahmed A. Moustafa. “A Computational Model of Pattern Separation Efficiency in the Dentate Gyrus with Implications in Schizophrenia.” *Frontiers in Systems Neuroscience* 9, no. Journal Article (2015): 42. <https://doi.org/10.3389/fnsys.2015.00042>.

Fricano-Kugler, Catherine J., Michael R. Williams, Bryan Luikart, Julia R. Salinaro, and Meijie Li. “Designing, Packaging, and Delivery of High Titer CRISPR Retro and Lentiviruses via Stereotaxic Injection.” *Journal of Visualized Experiments*, no. 111 (May 23, 2016): 53783. <https://doi.org/10.3791/53783>.

González-Burgos, I., D. A. Velázquez-Zamora, and C. Beas-Zárate. “Damage and Plasticity in Adult Rat Hippocampal Trisynaptic Circuit Neurons after Neonatal Exposure to Glutamate Excitotoxicity.” *International Journal of Developmental Neuroscience* 27, no. 8 (2009): 741–45. <https://doi.org/10.1016/j.ijdevneu.2009.08.016>.

GoodSmith, Douglas, Xiaojing Chen, Cheng Wang, Sang Hoon Kim, Hongjun Song, Andrea Burgalossi, Kimberly M. Christian, and James J. Knierim. “Spatial Representations of Granule Cells and Mossy Cells of the Dentate Gyrus.” *Neuron* 93, no. 3 (2017): 677-690.e5. <https://doi.org/10.1016/j.neuron.2016.12.026>.

Gupta, Akshay, Deepak Subramanian, Archana Proddutur, Yun-Juan Chang, Jenieve Guevarra, Yash Shah, Fatima S. Elgammal, and Vijayalakshmi Santhakumar. “Semilunar Granule Cells Maintain Distinct Dendritic Morphology and Inhibition through Postnatal Development and Receive Heightened Inhibition in Adolescence.” *BioRxiv*, January 1, 2019, 2019.12.17.880005. <https://doi.org/10.1101/2019.12.17.880005>.

- Gupta, Akshay, Fatima S. Elgammal, Archana Proddutur, Samik Shah, and Vijayalakshmi Santhakumar. “Decrease in Tonic Inhibition Contributes to Increase in Dentate Semilunar Granule Cell Excitability after Brain Injury.” *The Journal of Neuroscience : The Official Journal of the Society for Neuroscience* 32, no. 7 (2012): 2523–37.
<https://doi.org/10.1523/JNEUROSCI.4141-11.2012>.
- Hatami, Maryam, Sabine Conrad, Pooyan Naghsh, Gonzalo Alvarez-Bolado, and Thomas Skutella. “Cell-Biological Requirements for the Generation of Dentate Gyrus Granule Neurons.” *Frontiers in Cellular Neuroscience* 12, no. Journal Article (2018): 402.
<https://doi.org/10.3389/fncel.2018.00402>.
- Henze, D.A, N.N Urban, and German Barrionuevo. “The Multifarious Hippocampal Mossy Fiber Pathway: A Review.” *Neuroscience* 98, no. 3 (2000): 407–27. [https://doi.org/10.1016/S0306-4522\(00\)00146-9](https://doi.org/10.1016/S0306-4522(00)00146-9).
- Houser, Carolyn R. “Interneurons of the Dentate Gyrus: An Overview of Cell Types, Terminal Fields and Neurochemical Identity.” In *Progress in Brain Research*, 163:217–811. Elsevier, 2007. [https://doi.org/10.1016/S0079-6123\(07\)63013-1](https://doi.org/10.1016/S0079-6123(07)63013-1).
- Jinde, Seiichiro, Veronika Zsiros, and Kazu Nakazawa. “Hilar Mossy Cell Circuitry Controlling Dentate Granule Cell Excitability.” *Frontiers in Neural Circuits* 7, no. Journal Article (2013): 14. <https://doi.org/10.3389/fncir.2013.00014>.
- Kaptan, Zülal, and Gülay Üzümlü. “The Role of Adult Hippocampal Neurogenesis in Learning and Memory Function.” *Turkish Journal Of Neurology* 22, no. 4 (2016): 149–55.
<https://doi.org/10.4274/tnd.68889>.
- Kerloch, Thomas, Solène Clavreul, Adeline Goron, Djoher Nora Abrous, and Emilie Pacary. “Dentate Granule Neurons Generated During Perinatal Life Display Distinct Morphological

- Features Compared With Later-Born Neurons in the Mouse Hippocampus.” *Cerebral Cortex* 29, no. 8 (July 22, 2019): 3527–39. <https://doi.org/10.1093/cercor/bhy224>.
- Kumar A, Pareek V, Faiq MA, Ghosh SK, Kumari C. Adult Neurogenesis in Humans: A Review of Basic Concepts, History, Current Research, and Clinical Implications. *Innov Clin Neurosci*. 2019 May 1;16(5-6):30-37.
- Larimer, Phillip, and Ben W. Strowbridge. “Representing Information in Neuronal Cell Assemblies: Persistent Activity in the Dentate Gyrus Mediated by Semilunar Granule Cells.” *Nature Neuroscience* 13, no. 2 (2010): 213–22. <https://doi.org/10.1038/nn.2458>.
- Mendoza, John, Anne Foundas, and SpringerLink (Online service). *Clinical Neuroanatomy: A Neurobehavioral Approach*. 1st 2008. Book, Whole. New York, NY: Springer New York, 2008.
- Rovira-Esteban, Laura, Norbert Hájos, Gergő Attila Nagy, Carlos Crespo, Juan Nacher, Emilio Varea, and José Miguel Blasco-Ibáñez. “Semilunar Granule Cells Are the Primary Source of the Perisomatic Excitatory Innervation onto Parvalbumin-Expressing Interneurons in the Dentate Gyrus.” *Eneuro* 7, no. 4 (July 2020): ENEURO.0323-19.2020. <https://doi.org/10.1523/ENEURO.0323-19.2020>.
- Sancho-Bielsa, Francisco J., Juan D. Navarro-López, Gregori Alonso-Llosa, Asunción Molowny, Xavier Ponsoda, Javier Yajeya, and Carlos López-García. “Neurons of the Dentate Molecular Layer in the Rabbit Hippocampus.” *PloS One* 7, no. 11 (2012): e48470. <https://doi.org/10.1371/journal.pone.0048470>.
- Save, Laurène, Agnès Baude, and Rosa Cossart. “Temporal Embryonic Origin Critically Determines Cellular Physiology in the Dentate Gyrus.” *Cerebral Cortex* 29, no. 6 (2019): 2639–52. <https://doi.org/10.1093/cercor/bhy132>.

- Scharfman, Helen E. “Advances in Understanding Hilar Mossy Cells of the Dentate Gyrus.” *Cell and Tissue Research* 373, no. 3 (2018): 643–52. <https://doi.org/10.1007/s00441-017-2750-5>.
- Scharfman, Helen E. “Epileptogenesis in the Parahippocampal Region: Parallels with the Dentate Gyrus.” *Annals of the New York Academy of Sciences* 911, no. 1 (2000): 305–27. <https://doi.org/10.1111/j.1749-6632.2000.tb06734.x>.
- Scharfman, Helen E. “The Enigmatic Mossy Cell of the Dentate Gyrus.” *Nature Reviews. Neuroscience* 17, no. 9 (2016): 562–75. <https://doi.org/10.1038/nrn.2016.87>.
- Scharfman, Helen E. “The Neurobiology of Epilepsy.” *Current Neurology and Neuroscience Reports* 7, no. 4 (July 2007): 348–54. <https://doi.org/10.1007/s11910-007-0053-z>.
- Scharfman, Helen E., and Hannah L. Bernstein. “Potential Implications of a Monosynaptic Pathway from Mossy Cells to Adult-Born Granule Cells of the Dentate Gyrus.” *Frontiers in Systems Neuroscience* 9, no. Journal Article (2015): 112. <https://doi.org/10.3389/fnsys.2015.00112>.
- Schmidt-Hieber, Christoph, Peter Jonas, and Josef Bischofberger. “Enhanced Synaptic Plasticity in Newly Generated Granule Cells of the Adult Hippocampus.” *Nature* 429, no. 6988 (May 2004): 184–87. <https://doi.org/10.1038/nature02553>.
- Schmidt, Brandy, Diano F. Marrone, and Etan J. Markus. “Disambiguating the Similar: The Dentate Gyrus and Pattern Separation.” *Behavioural Brain Research* 226, no. 1 (2012): 56–65. <https://doi.org/10.1016/j.bbr.2011.08.039>.
- Senzai, Yuta. “Function of Local Circuits in the Hippocampal Dentate Gyrus-CA3 System.” *Neuroscience Research* 140, no. Journal Article (2019): 43–52. <https://doi.org/10.1016/j.neures.2018.11.003>.

- Sik, Attila, Markku Penttonen, and György Buzsáki. “Interneurons in the Hippocampal Dentate Gyrus: An In Vivo Intracellular Study.” *European Journal of Neuroscience* 9, no. 3 (1997): 573–88. <https://doi.org/10.1111/j.1460-9568.1997.tb01634.x>.
- Stepan, Jens, Julien Dine, Thomas Fenzl, Stephanie A. Polta, Gregor von Wolff, Carsten T. Wotjak, and Matthias Eder. “Entorhinal Theta-Frequency Input to the Dentate Gyrus Trisynaptically Evokes Hippocampal CA1 LTP.” *Frontiers in Neural Circuits* 6, no. Journal Article (2012): 64. <https://doi.org/10.3389/fncir.2012.00064>.
- Sun, Yanjun, Steven F. Grieco, Todd C. Holmes, and Xiangmin Xu. “Local and Long-Range Circuit Connections to Hilar Mossy Cells in the Dentate Gyrus.” *ENeuro* 4, no. 2 (2017): ENEURO.0097-17.2017. <https://doi.org/10.1523/ENeuro.0097-17.2017>.
- Takarae, Yukari, and John Sweeney. “Neural Hyperexcitability in Autism Spectrum Disorders.” *Brain Sciences* 7, no. 10 (2017): 129. <https://doi.org/10.3390/brainsci7100129>.
- Tamir, Idit, Moshe Daninos, and Yoel Yaari. “Plasticity of Intrinsic Firing Response Gain in Principal Hippocampal Neurons Following Pilocarpine-Induced Status Epilepticus.” *Neuroscience* 357, no. Journal Article (2017): 325–37. <https://doi.org/10.1016/j.neuroscience.2017.06.013>.
- Tang, Jonathan Cy, Eugene Drokhlyansky, Behzad Etemad, Stephanie Rudolph, Binggege Guo, Sui Wang, Emily G. Ellis, Jonathan Z. Li, and Constance L. Cepko. “Detection and Manipulation of Live Antigen-Expressing Cells Using Conditionally Stable Nanobodies.” *ELife* 5, no. Journal Article (2016). <https://doi.org/10.7554/eLife.15312>.
- Walker, Matthew C., Ivan Pavlov, and Dimitri M. Kullmann. “A ‘sustain Pedal’ in the Hippocampus?” *Nature Neuroscience* 13, no. 2 (2010): 146.

- Wang, Guohua, Canmao Wang, He Chen, Limei Chen, and Juan Li. “Activation of 6–8-Week-Old New Mature Adult-Born Dentate Granule Cells Contributes to Anxiety-like Behavior.” *Neurobiology of Stress* 15 (November 2021): 100358.
<https://doi.org/10.1016/j.ynstr.2021.100358>.
- Williams, Philip A., Phillip Larimer, Yuan Gao, and Ben W. Strowbridge. “Semilunar Granule Cells: Glutamatergic Neurons in the Rat Dentate Gyrus with Axon Collaterals in the Inner Molecular Layer.” *Journal of Neuroscience* 27, no. 50 (2007): 13756–61.
<https://doi.org/10.1523/JNEUROSCI.4053-07.2007>.
- Woods, Nicholas I., Fabio Stefanini, Daniel L. Apodaca-Montano, Isabelle M.C. Tan, Jeremy S. Biane, and Mazen A. Kheirbek. “The Dentate Gyrus Classifies Cortical Representations of Learned Stimuli.” *Neuron* 107, no. 1 (July 2020): 173-184.e6.
<https://doi.org/10.1016/j.neuron.2020.04.002>.
- Xiong, Guoxiang, Hannah Metheny, Brian N. Johnson, and Akiva S. Cohen. “A Comparison of Different Slicing Planes in Preservation of Major Hippocampal Pathway Fibers in the Mouse.” *Frontiers in Neuroanatomy* 11, no. Journal Article (2017): 107.
<https://doi.org/10.3389/fnana.2017.00107>.
- Xu, Wenhua, Hui Li, Caigu He, Jacqueline Frank, and Gang Chen. “Early Ethanol Exposure Inhibits the Differentiation of Hippocampal Dentate Gyrus Granule Cells in a Mouse Model of Fetal Alcohol Spectrum Disorders.” *Alcoholism: Clinical and Experimental Research* 44, no. 5 (2020): 1112–22. <https://doi.org/10.1111/acer.14330>.
- Yu, Diana X., Maria C. Marchetto, and Fred H. Gage. “How to Make a Hippocampal Dentate Gyrus Granule Neuron.” *Development (Cambridge, England)* 141, no. 12 (2014): 2366–75.
<https://doi.org/10.1242/dev.096776>.